The Bell System Technical Journal
Vol. 53, No. 5, May–June 1974
Printed in U.S.A.

Finite-Element Method for the Determination of Thermal Stresses in Anisotropic Solids of Revolution

By S. KAUFMAN

(Manuscript received October 19, 1973)

This paper discusses stresses and deflections in anisotropic solid structures of revolution. It presents two methods based on finite-element techniques: one, a solid-of-revolution method in which material properties, applied forces, and temperatures are independent of angle, and two, a long-cylinder method in which these properties are independent of the longitudinal coordinate. These methods are postulated on uniform stress fields within the element, rather than on the usual functional displacement description within the element. A Fortran program has been written for both these methods, and ample test problems are presented to validate the methods. An application is presented for thermal stresses induced during the post-growth cooling stage of Czochralski-grown lithium tantalate crystals.

I. INTRODUCTION

This paper considers two finite-element networks. The first network consists of triangular annuli forming a solid of revolution of any arbitrary cross section in the radial-longitudinal plane. The network has 2π symmetry with regard to material properties, external loadings, and temperatures. The second network consists of trapezoidal and triangular elements in the plane of the circle forming a right circular (actually, a polygon cross section) cylinder long in the longitudinal direction. The restriction of 2π symmetry is lifted for the second network and is replaced with the restriction that material properties, external loadings, and temperatures are independent of the longitudinal direction of the cylinder.

Both methods were programmed on the IBM 370 computer. For the first method, two test plane strain problems are presented: one, a hollow cylinder subjected to a negative radial pressure and two, a

solid cylinder subjected to a linear radial temperature gradient. Comparisons of stresses and deflections with known plane strain solutions are excellent in both cases. In the second method, the solution of a long cylinder subjected to a linear radial thermal gradient is presented. Comparison with a known theoretical solution again was excellent.

Results are presented for thermal stresses induced in a lithium tantalate crystal during the post-growth cooling stage. Lithium tantalate is in crystal class C_{3v}. By aligning the trigonal axis of the crystal with the longitudinal axis of the cylinder, the problem can be analyzed by both methods. Comparison of thermal stresses obtained from the two methods was very good.

II. SOLID-OF-REVOLUTION METHOD

The basic element for this method is the triangular annulus shown in Fig. 1. The element, defined in the radial-longitudinal plane $(r - z)$, has 2π symmetry. A network of these elements will comprise any desired solid of revolution, whether it is solid or hollow, cylindrical or conical, or any combination thereof. Material properties, temperature distributions, and external forces must be independent of angle. The material properties are then limited to an orthotropic system with isotropic properties in the plane of the circle. This limitation is lifted in the case of the long cylinder method presented in the next section.

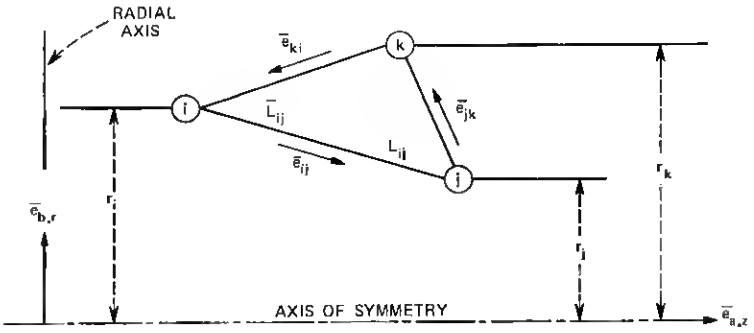

$$\bar{A} = \tfrac{1}{2}\bar{L}_{ij} \times \bar{L}_{jk} \qquad A = |A|$$

$$V = 2\pi A(r_i + r_j + r_k)/3$$

$$\bar{e}_{ij} = \bar{L}_{ij}/L_{ij}$$

$$A_{ij} = V/L_{ij} \quad [\text{HALF ALTITUDE AREA (k TO ij)}]$$

$$a_{ij} = \bar{e}_{ij} \cdot \bar{e}_a \qquad b_{ij} = \bar{e}_{ij} \cdot \bar{e}_b$$

Fig. 1—Properties of triangular annulus.

Solid triangular elements have heen used successfully by other authors;[1,2] however, a different approach is presented here. Rather than to assume a displacement function,[1,2] a simpler and more direct approach is to postulate uniform stress fields in the annulus. Tbis metbod was applied successfully in the mid-60's hy David B. Hall for tbe triangular membrane, but unfortunately his work has not been puhlished. Hall's triangular membrane is extended here to a three-dimensional model by incorporating a uniform hoop stress in the annulus.

The initial strategy is to relate equilihrium hetween forces at the three points of the triangle i, j, k, and stress fields parallel to the sides of the triangle σ_{ij}, σ_{jk}, σ_{ki}, and the hoop stress σ_θ. Before we do this, let us first compute a few properties of the triangular annulus. These properties include the area of the triangle A, length of each side L_{ij}, etc., volume V, areas A_{ij}, etc. associated with the stress fields σ_{ij}, etc., and direction cosines a_{ij}, b_{ij}, etc. These properties are presented in Fig. 1.

In matrix notation, equilihrium for annulus n hetween grid point forces and the four stress fields described ahove is given as follows.

$$\{F_n\} = [B]\{\sigma_o\}, \tag{1}$$

where

$$\{F_n\} = \{F_{ir}F_{iz}F_{jr}F_{jz}F_{kr}F_{kz}\},$$
$$\{\sigma_o\} = \{\sigma_{ij}\sigma_{jk}\sigma_{ki}\sigma_\theta\},$$

and

$$[B] = \begin{bmatrix} -A_{ij}b_{ij} & 0 & A_{ki}b_{ki} & 2\pi A/3 \\ -A_{ij}a_{ij} & 0 & A_{ki}a_{ki} & 0 \\ A_{ij}b_{ij} & -A_{jk}b_{jk} & 0 & 2\pi A/3 \\ A_{ij}a_{ij} & -A_{jk}a_{jk} & 0 & 0 \\ 0 & A_{jk}b_{jk} & -A_{ki}b_{ki} & 2\pi A/3 \\ 0 & A_{jk}a_{jk} & -A_{ki}a_{ki} & 0 \end{bmatrix}.$$

The r and z subscripts attached to the forces F_{ir}, F_{iz}, etc. refer to the radial and longitudinal directions, respectively.

The skew stress field σ_{ij}, σ_{jk}, σ_{ki} is merely an artifice to allow us to readily establish the equilihrium relationship. We are actually interested in tbe orthogonal field σ_z, σ_r, τ_{rz}, as shown in Fig. 2. The relationship hetween the two fields including the hoop stress is given helow.

$$\{\sigma_n\} = [D]\{\sigma_0\}, \tag{2}$$

wbere

$$\{\sigma_n\} = \{\sigma_z\sigma_r\tau_{rz}\sigma_\theta\}$$

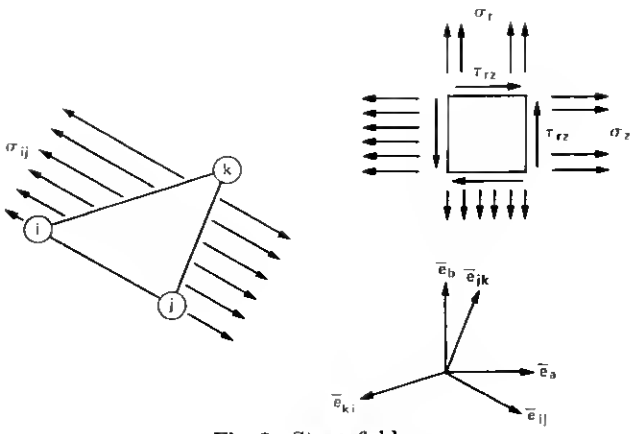

Fig. 2—Stress fields.

and

$$[D] = \begin{bmatrix} a_{ij}^2 & a_{jk}^2 & a_{ki}^2 & 0 \\ b_{ij}^2 & b_{jk}^2 & b_{ki}^2 & 0 \\ a_{ij}b_{ij} & a_{jk}b_{jk} & a_{ki}b_{ki} & 0 \\ 0 & 0 & 0 & 1 \end{bmatrix}.$$

After inverting eq. (2) and substituting it into eq. (1), the following relationship is obtained.

$$\{F_n\} = [F]\{\sigma_n\}, \tag{3}$$

where

$$[F] = [B][D]^{-1}.$$

A conjugate relationship to eq. (3) by an application of the principle of virtual work can be stated as

$$\{\epsilon_n\} = \frac{1}{V}[F]^t\{U_n\}, \tag{4}$$

where the strains are

$$\{\epsilon_n\} = \{\epsilon_z \epsilon_r \gamma_{rz} \epsilon_\theta\},$$

the deflections conjugate to $\{F_n\}$ are

$$\{U_n\} = \{U_{iz}U_{ir}U_{jr}U_{jz}U_{kr}U_{kz}\},$$

and the superscript t denotes a transposition.

The stress-strain relationship, including the thermal strains $\int \alpha dT$, is given as

$$\{\sigma_n\} = [C]\left(\{\epsilon_n\} - \left\{\int \alpha dT\right\}\right), \tag{5}$$

where $[C]$ is a symmetric 4×4 stress-strain matrix such that

$$C_{11} = C_{12}, \quad C_{14} = C_{24}, \quad C_{13} = C_{23} = C_{43} = 0,$$

and

$$\left\{\int \alpha dT\right\} = \left\{\int \alpha_z dT \int \alpha_r dT \; 0 \int \alpha_\theta dT\right\}, \quad \alpha_r = \alpha_\theta.$$

Substituting eq. (5) into eq. (4) obtains the stresses in terms of the unknown deflections and known thermal strains as

$$\{\sigma_n\} = [C]\left(\frac{1}{V}[F]^t\{U_n\} - \left\{\int \alpha dT\right\}\right). \tag{6}$$

Substituting eq. (6) into eq. (3) obtains contributions to the network stiffness matrix and thermal load vector for annulus n or

$$\{F_n\} = [K_n]\{U_n\} - \{E_n\}, \tag{7}$$

where

$$[K_n] = \frac{1}{V}[F][C][F]^t$$

is a symmetric 6×6 stiffness matrix and

$$\{E_n\} = [F][C]\left\{\int \alpha dT\right\}$$

is a 6×1 thermal load vector.

Annuli contributions to the network stiffness matrix and thermal load vector are additive, and hence eq. (7) can he written for the network as

$$\{F\} = [K]\{U\} - \{E\}, \tag{7a}$$

where

$$[K] = \sum_n [K_n] \quad \text{and} \quad \{E\} = \sum_n \{E_n\},$$

and where the number of equations equals twice the number of points of the network (one longitudinal and one radial degree of freedom per point).

The $[K]$ matrix in eq. (7a) is singular, as there is no constraint to prevent rigid body motion in the longitudinal direction. Rigid-body motion in the radial direction is prevented by the hoop stress field, as can be seen in eq. (1). (Note that in Eq. (1) σ_θ is the only non-self-equilibrating stress field.) In addition to at least one reference longitudinal constraint, radial constraints must be provided for solid cylinders at points of zero radius to prevent radial (or hoop) motions at these singularities. The degrees of freedom can now be partitioned

into an unconstrained set denoted by "a" and a constrained set denoted by "b." This partitioning can be represented schematically as

$$\begin{Bmatrix} F_a \\ F_b \end{Bmatrix} = \begin{bmatrix} K_{aa} K_{ab} \\ K_{ab}^t K_{bb} \end{bmatrix} \begin{Bmatrix} U_a \\ U_b = 0 \end{Bmatrix} - \begin{Bmatrix} E_a \\ E_b \end{Bmatrix}. \tag{8}$$

From the upper equation of (8), the previously unknown deflections can now be obtained in terms of known external forces and thermal loads, or

$$\{U_a\} = [K_{aa}]^{-1}(\{F_a\} + \{E_a\}). \tag{9}$$

From the lower equation of (8) and with the help of eq. (9), the forces of constraint, if desired, can be obtained as

$$\{F_b\} = [K_{ab}]^t[K_{aa}]^{-1}\{F_a\} - \{F_b^*\} - (\{E_b\} - [K_{ab}]^t[K_{aa}]^{-1}\{E_a\}), \tag{9a}$$

where $\{F_b^*\}$ represents external forces applied at the constraint points.

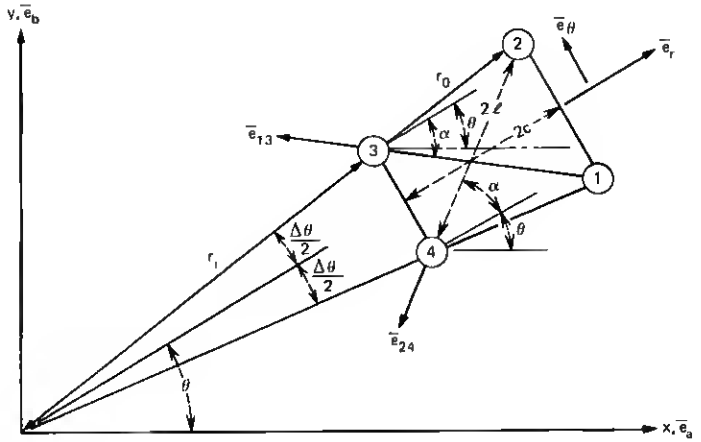

$\alpha = \tan^{-1}[(r_0+r_i)\sin\frac{\Delta\theta}{2}/(r_0-r_i)]$ $\quad a_r = \bar{e}_r\cdot\bar{e}_a$ $\quad b_r = \bar{e}_r\cdot\bar{e}_b$

$\bar{e}_{13} = [-\cos(\alpha-\theta)\bar{e}_a, \sin(\alpha-\theta)\bar{e}_b]$ $\quad a_\theta = \bar{e}_\theta\cdot\bar{e}_a$ $\quad b_\theta = \bar{e}_\theta\cdot\bar{e}_b$

$\bar{e}_{24} = [-\cos(\alpha+\theta)\bar{e}_a, -\sin(\alpha+\theta)\bar{e}_b]$ $\quad a_{13} = \bar{e}_{13}\cdot\bar{e}_a$ $\quad b_{13} = \bar{e}_{13}\cdot\bar{e}_b$

$2\ell = [\sin^2\frac{\Delta\theta}{2}(r_0+r_i)^2 + (r_0+r_i)^2]^{1/2}$ $\quad a_{24} = \bar{e}_{24}\cdot\bar{e}_a$ $\quad b_{24} = \bar{e}_{24}\cdot\bar{e}_b$

$\bar{e}_r = (\cos\theta\,\bar{e}_a, \sin\theta\,\bar{e}_b)$ $\quad A = (r_0-r_i)(r_0+r_i)\sin\frac{\Delta\theta}{2}\cos\frac{\Delta\theta}{2}$ (AREA)

$\bar{e}_\theta = (-\sin\theta\,\bar{e}_a, \cos\theta\,\bar{e}_b)$ $\quad 2c = (r_0-r_i)\cos\frac{\Delta\theta}{2}$ $\quad f = A/4c$

Fig. 3—Properties of the trapezoidal element.

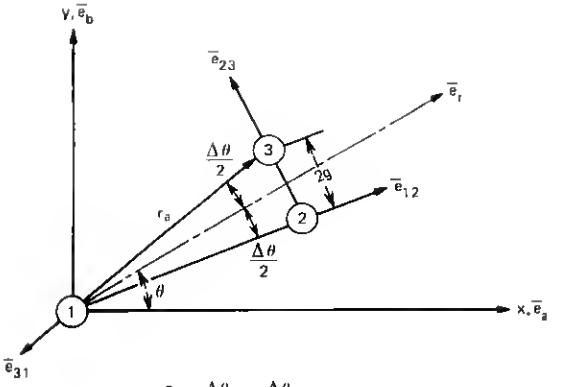

$$A = r_a^2 \sin\frac{\Delta\theta}{2} \cos\frac{\Delta\theta}{2} \text{ (AREA)}$$

$$2g = r_a \sin\Delta\theta$$

$$\bar{e}_{12} = [\cos(\theta - \frac{\Delta\theta}{2})\,\bar{e}_a, \sin(\theta - \frac{\Delta\theta}{2})\,\bar{e}_b]$$

$$a_{12} = \bar{e}_{12} \cdot \bar{e}_a \qquad b_{12} = \bar{e}_{12} \cdot \bar{e}_b$$

$$\bar{e}_{23} = (-\sin\theta\,\bar{e}_a, \cos\theta\,\bar{e}_b)$$

$$a_{23} = \bar{e}_{23} \cdot \bar{e}_a \qquad b_{23} = \bar{e}_{23} \cdot \bar{e}_b$$

$$\bar{e}_{31} = [-\cos(\theta + \frac{\Delta\theta}{2})\,\bar{e}_a, -\sin(\theta + \frac{\Delta\theta}{2})\,\bar{e}_b]$$

$$a_{31} = \bar{e}_{31} \cdot \bar{e}_a \qquad b_{31} = \bar{e}_{31} \cdot \bar{e}_b$$

Fig. 4—Properties of the triangular element.

III. LONG-CYLINDER METHOD

In this section, tbe 2π symmetry requirements as to material properties, external loadings, and temperature are lifted and a two-dimensional model is constructed in the plane of the circle. Tbe cylinder is considered long in the z-(longitudinal) direction and material properties, external loadings, and temperatures are assumed independent of z. Shear stresses τ_{yz} and τ_{zz} are assumed to be zero. The most general stress-strain relationship considered is tbe 4×4 submatrix bounded by tbe dashed lines of eq. (18) (appendix) with the additional proviso of no coupling between the stresses σ_z, σ_y, σ_x, τ_{xy} and the strains γ_{yz}, γ_{zx}. Tentatively, we let ϵ_z vanish during the initial pbase of the analysis. This restriction is subsequently removed in a manner similar to that described by Timoshenko[3] for long isotropic cylinders.

The hasic building blocks of the long cylinder is the trapezoidal element (Fig. 3) and the isosceles triangular element (Fig. 4, solid cylinders only). The trapezoidal element is subjected to three constant

stress fields: a radial stress σ_r, a tangential stress σ_θ, and a shear stress $\tau_{r\theta}$. Tbe triangular element is likewise subjected to three uniform stress fields, each parallel to a side of the triangle. Equilibrium between forces collected at tbe apices of the elements and tbree uniform stress fields are obtained as shown below (see Figs. 3 and 4 for the properties of the elements).

Trapezoid:

$$\begin{Bmatrix} F_{x1} \\ F_{y1} \\ F_{x2} \\ F_{y2} \\ F_{x3} \\ F_{y3} \\ F_{x4} \\ F_{y4} \end{Bmatrix} = \begin{bmatrix} fa_r & -ca_\theta & la_{13} \\ fb_r & -cb_\theta & lb_{13} \\ fa_r & ca_\theta & -la_{24} \\ fb_r & cb_\theta & -lb_{24} \\ -fa_r & ca_\theta & -la_{13} \\ -fb_r & cb_\theta & -lb_{13} \\ -fa_r & -ca_\theta & la_{24} \\ -fb_r & -cb_\theta & la_{24} \end{bmatrix} \begin{Bmatrix} \sigma_r \\ \sigma_\theta \\ \tau_{r\theta} \end{Bmatrix}. \tag{10}$$

Triangle:

$$\begin{Bmatrix} F_{x1} \\ F_{y1} \\ F_{x2} \\ F_{y2} \\ F_{x3} \\ F_{y3} \end{Bmatrix} = \begin{bmatrix} -ga_{12} & 0 & ga_{31} \\ -gb_{12} & 0 & gb_{31} \\ ga_{12} & -r_a/2 & 0 \\ gb_{12} & -r_a/2 & 0 \\ 0 & r_a/2 & -ga_{31} \\ 0 & r_a/2 & -gb_{31} \end{bmatrix} \begin{Bmatrix} \sigma_{12} \\ \sigma_{23} \\ \sigma_{31} \end{Bmatrix}. \tag{11}$$

The relationship between the orthogonal stress field ($\sigma_r \sigma_\theta \tau_{r\theta}$) and the skew stress field ($\sigma_{12}\ \sigma_{23}\ \sigma_{31}$) is given below for the triangle.

$$\{\sigma_b\} = \begin{Bmatrix} \sigma_r \\ \sigma_\theta \\ \tau_{r\theta} \end{Bmatrix}$$

$$= \begin{bmatrix} \cos^2 \Delta\theta/2 & 0 & \cos^2 \Delta\theta/2 \\ \sin^2 \Delta\theta/2 & 1 & \sin^2 \Delta\theta/2 \\ -\sin \Delta\theta/2 \cos \Delta\theta/2 & 0 & \sin \Delta\theta/2 \cos \Delta\theta/2 \end{bmatrix} \begin{Bmatrix} \sigma_{12} \\ \sigma_{23} \\ \sigma_{31} \end{Bmatrix}. \tag{11a}$$

After inverting eq. (11a) and substituting it into eq. (11), equilibrium is established between tbe orthogonal stress field and tbe forces (denoted as $\{F_n\}$) at the apices of the element or the points of tbe network. Denote this relationsbip as:

$$\{F_n\} = [H_n]\{\sigma_b\}. \tag{12}$$

Similarly, for the trapezoid, eq. (12) will be the sborthand matrix notation for eq. (10).

Conjugate to the forces $\{F_n\}$ are deflections $\{U_n\}$ and therefore the conjugate relationship to eq. (12) can be constructed as

$$\{\epsilon_b\} = 1/A[H_n]^t\{U_n\}, \tag{13}$$

where A is the volume (area times unit thickness) of the trapezoid or triangle.

Upon substituting eq. (13) into eq. (26), the stresses in the element in terms of the unknown deflections at the apices and the known thermal strains are obtained.

$$\{\sigma_b\} = [C]\left(1/A[H_n]^t\{U_n\} - [B_b]\left\{\int \alpha dT\right\}\right). \tag{14}$$

Upon substituting eq. (14) into eq. (12), contributions to the network stiffness matrix and thermal load vector are obtained for the element

$$\{F_n\} = [K_n]\{U_n\} - \{E_n\}, \tag{15}$$

where

$$[K_n] = 1/A[H_n][C][H_n]^t$$

is a symmetric 8×8 or 6×6 stiffness matrix and

$$\{E_n\} = [H_n][C][E_b]\left\{\int \alpha dT\right\}$$

is an 8×1 or 6×1 thermal load vector.

Contributions of each element to the network stiffness matrix and thermal load vector are additive, and hence eq. (7a) can represent the force balance at all the points of the long-cylinder network as well as those of the solid-of-revolution network.

Noting the material restrictions outlined in the beginning of this section, a network of triangles and trapezoids need only occupy one-quarter of a circle with planes of symmetry at $\theta = 0$ and $\pi/2$. Hence, tangential deflections must vanish at all points along these planes. The previously unknown deflections and constraint forces can now be solved in terms of known external forces and thermal loads in the same manner as was accomplished in the preceding section [see eqs. (8), (9), and (9a)].

We are not quite finished. Recall that we have let $\epsilon_z = 0$ throughout the cylinder, resulting in an axial stress σ_z [eq. (23)] applied to the ends of the cylinder. If we superimpose a uniform axial stress $\langle\sigma_z\rangle$ such that the resulting force on the ends of the cylinder is zero, the self-equilibrating distribution remaining on the ends will, by St. Venant's principle,[3] give rise only to local effects at the ends. The uni-

form axial stress correction to be added to eq. (23) is given as

$$\langle \sigma_z \rangle = - \frac{\int \sigma_z \, [\text{eq. (23)}] dA}{\int dA}. \tag{16}$$

This correction results in added radial and tangential strains obtained from eq. (22).

$$\langle \epsilon_r(\theta) \rangle = E_{13}(\theta) \langle \sigma_z \rangle = (E_{zz} \cos^2\theta + E_{yz} \sin^2\theta) \langle \sigma_z \rangle \tag{16a}$$

$$\langle \epsilon_\theta(\theta) \rangle = E_{23}(\theta) \langle \sigma_z \rangle = (E_{zz} \sin^2\theta + E_{yz} \cos^2\theta) \langle \sigma_z \rangle. \tag{16b}$$

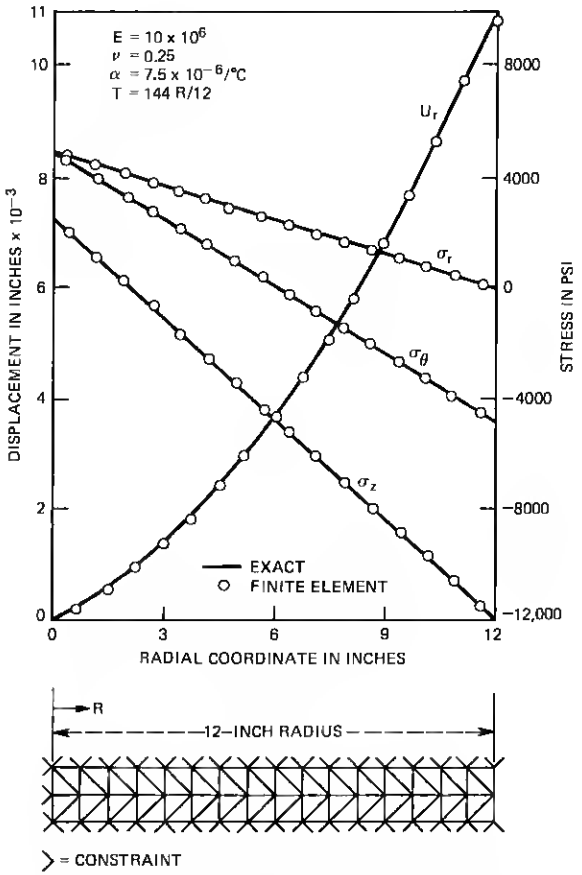

Fig. 5—Thermal stresses plane strain problem.

The resulting correction to the radial and tangential deflections are next obtained.

$$\langle U_r(r, \theta)\rangle = r\langle \epsilon_r(\theta)\rangle = r(E_{xy}\cos^2\theta + E_{yz}\sin^2\theta)\langle \sigma_z\rangle \tag{17}$$

$$\langle U_\theta(r, \theta)\rangle = \int_0^\theta (r\langle \epsilon_\theta(\theta)\rangle - \langle U_r(r, \theta)\rangle)d\theta$$

$$= r\int^\theta (E_{23}(\theta) - E_{13}(\theta))\langle \sigma_z\rangle d\theta$$

$$= r\sin\theta\cos\theta\,(E_{yz} - E_{xz}). \tag{17a}$$

Note that the correction $\langle U_\theta(r, \theta)\rangle$ vanishes at $\theta = 0$ and $\theta = \pi/2$, agreeing with the stipulated boundary conditions stated previously.

IV. COMPARISONS WITH THEORETICAL SOLUTIONS

Two plane strain problems are presented for the solid-of-revolution method: one, a linear radial thermal gradient applied to an isotropic solid cylinder (Fig. 5) and two, a negative pressure applied to the outside circumference of a hollow cylinder (Fig. 6). Comparisons were

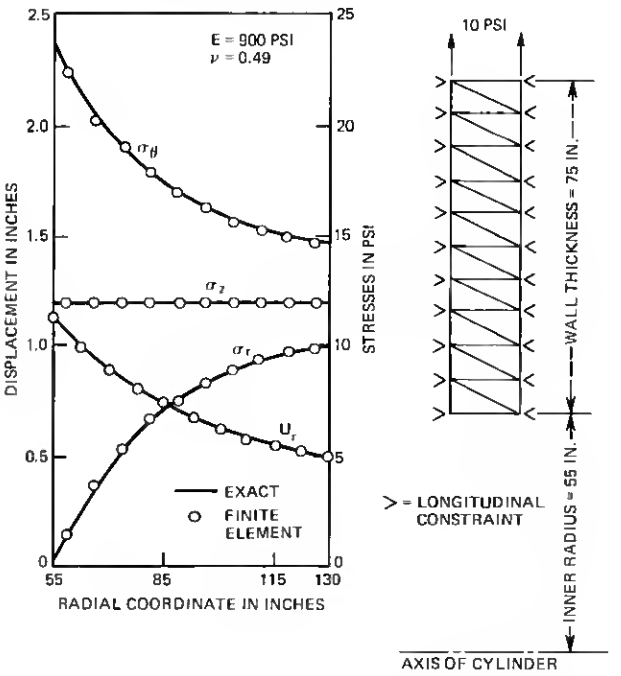

Fig. 6—Plane strain solution—thick-walled cylinder.

made of the finite element computer results with known theoretical[3] solutions. The agreement was excellent.

A thermal problem is presented for the long-cylinder method in which an isotropic cylinder is subjected to a constant temperature plus a radial thermal gradient (Fig. 7). Comparisons were made of the finite-element computer results with a known theoretical solution.[3] The known solution on page 410 of Ref. 3 was found to be in error. In the expression for radial displacement (U), insert $(1 - 3\nu)/(1 - \nu)$ for $(1 - 2\nu)$ and in the expression for σ_z, replace $2r$ with 2. After the above corrections were made to the theoretical solution, excellent comparisons resulted as shown in Fig. 7.

V. THERMAL STRESSES IN LITHIUM TANTALATE CRYSTALS

Thermal stresses were computed for a lithium tantalate crystal, class C_{3v}, during the post-growth cooling stage. The crystal was analyzed by the two methods presented in this paper on the IBM 370 computer. For the solid-of-revolution method (Fig. 8), the model con-

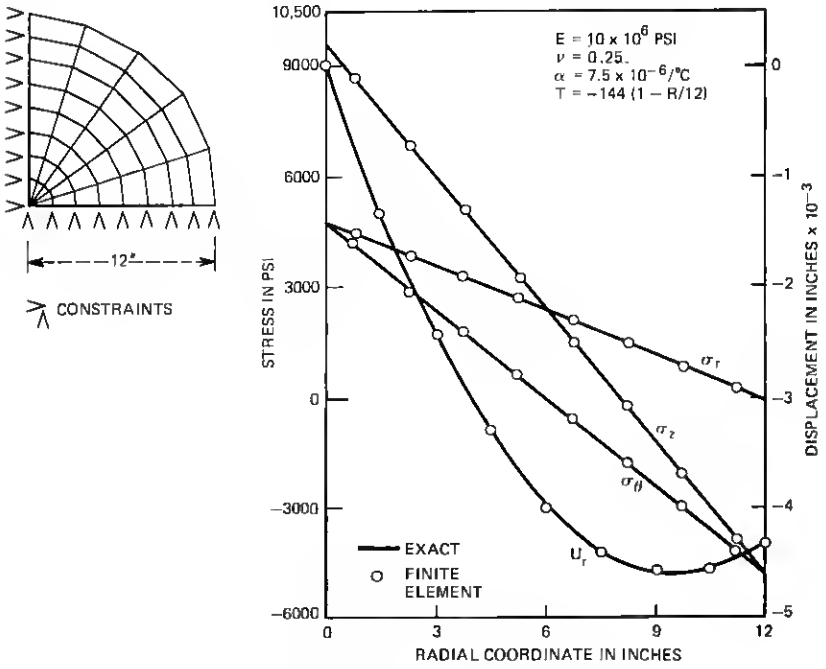

Fig. 7—Thermal stresses—long cylinder.

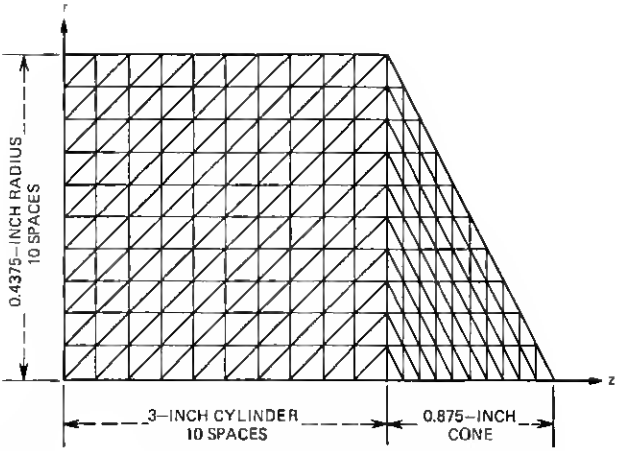

Fig. 8—Network of triangular annuli—lithium tantalate crystal—solid-of-revolution model.

sists of a right cylinder of radius $a = 0.4375$ inch and length $b = 3$ inches plus a cone of length 0.875 inch attached to the far (cold) end. Radial constraints are provided at all zero radius points. For the long-cylinder method (Fig. 9), the model comprises one-quarter of a circle with tangential constraints at all points along the two planes of symmetry ($\theta = 0$ and $\pi/2$).

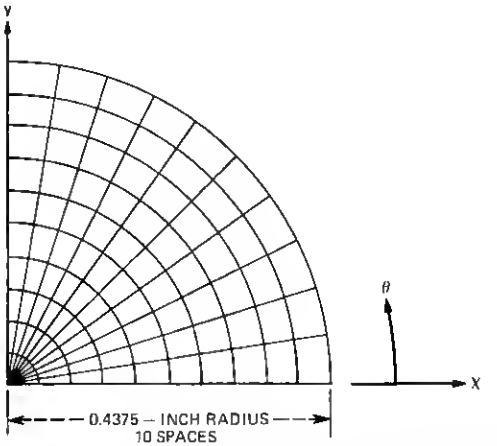

Fig. 9—Network of triangles and trapezoids—lithium tantalate crystal—long-cylinder model.

Elastic properties[4] of lithium tantalate are shown in Fig. 10. Axis 1 is perpendicular to the vertical mirror plane and axis 3 corresponds to the trigonal axis of the crystal. If we strike out the small shear coupling terms, c_{14}, in Fig. 10, then we have met the stress-strain relationship [eqs. (5) and (18)] requirements of this paper. The coefficients of thermal expansion will be assumed constant in the 1, 2 directions and piecewise linear along the trigonal axis 3. These coefficients[5] are given below.

$$\begin{aligned}
\alpha_1 = \alpha_2 &= 21.9 \times 10^{-6}/°C \\
\alpha_3 &= 8.35 \times 10^{-6}/°C \quad 625°C \text{ and higher} \\
&\quad -3.1 \times 10^{-6}/°C \quad 500°C - 625°C \\
&\quad 0 \quad 400°C - 500°C \\
&\quad 1.16 \times 10^{-6}/°C \quad \text{room temperature} - 400°C.
\end{aligned}$$

The crystal is assumed to be in a stress-free condition at an elevated temperature distribution $T1$, and elastic material behavior is assumed linear from the initial state of strain at temperature distribution $T1$ to the final state of stress and strain at room temperature (26°C). This assumption rules out plasticity and stress relaxation. It is felt that ignoring these nonlinear effects plus ignoring the initial state of stress at $T1$ does not distort the qualitative picture of the stress pattern after the cooling-down process. The elevated temperature distribution in degrees centigrade is given below.

$$\begin{aligned}
T1 &= 1500 - 100\,(r/a)^2 - 500\,z/b, \text{ for solid of revolution} \\
&= 1500 - 100\,(r/a)^2, \text{ for the long cylinder.}
\end{aligned}$$

The addition of the longitudinal gradient for the solid-of-revolution method was found to induce negligible stress in the crystal.

For the solid-of-revolution method (z-growth), material axes 1, 2, and 3 correspond to r, θ, and z, respectively. For the long-cylinder method, two cases were investigated: one, z-growth where material axes 1, 2, and 3 correspond to x, y, and z, respectively, and two, y-growth where material axes 1, 2, and 3 correspond to z, x, and y,

$$\begin{Bmatrix} \sigma_1 \\ \sigma_2 \\ \sigma_3 \\ \tau_{23} \\ \tau_{31} \\ \tau_{12} \end{Bmatrix} = \begin{bmatrix} c_{11} & c_{12} & c_{13} & \cancel{c_{14}} & 0 & 0 \\ c_{12} & c_{11} & c_{13} & \cancel{-c_{14}} & 0 & 0 \\ c_{13} & c_{13} & c_{33} & 0 & 0 & 0 \\ \cancel{c_{14}} & \cancel{-c_{14}} & 0 & c_{44} & 0 & 0 \\ 0 & 0 & 0 & 0 & c_{44} & \cancel{c_{14}} \\ 0 & 0 & 0 & 0 & \cancel{c_{14}} & c_{66} \end{bmatrix} \begin{Bmatrix} \epsilon_1 \\ \epsilon_2 \\ \epsilon_3 \\ \gamma_{23} \\ \gamma_{31} \\ \gamma_{12} \end{Bmatrix}$$

$c_{33} = 2.75 \times 10^{11}\ \text{N/m}^2$
$c_{11} = 2.33$
$c_{14} = 0.11$
$c_{12} = 0.47$
$c_{13} = 0.80$
$c_{44} = 0.94$
$c_{66} = 0.93 = \frac{1}{2}(c_{11} - c_{12})$

Fig 10—$LiTaO_3$ stress-strain.

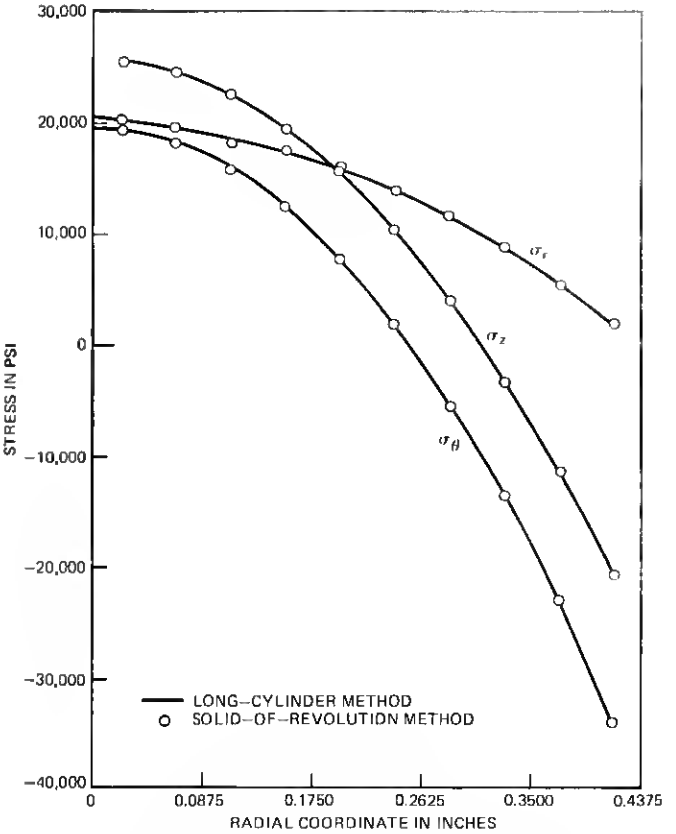

Fig. 11—Thermal stress comparison z-growth $LiTaO_3$ crystal.

respectively. A plot of thermal stresses for the z-growth crystals by both methods is compared in Fig. 11. Agreement is very good. A comparison of thermal stresses by the long-cylinder method of both z-growth and y-growth is shown in Fig. 12 at $\theta = 45°$. (Typically, θ-stress variations are less than 5 percent.) The maximum stress recorded in absolute value is about 39,000 psi for both z-growth and y-growth. The x-growth (material axis 3 corresponds to x) would yield the same results as y-growth. This can be inferred from examination of the material properties of Fig. 10.

VI. CONCLUSIONS

Excellent comparisons were obtained for stresses and deflection in isotropic cylinders between the methods described in this paper and known theoretical solutions (Figs. 5 to 7). Stress comparisons again

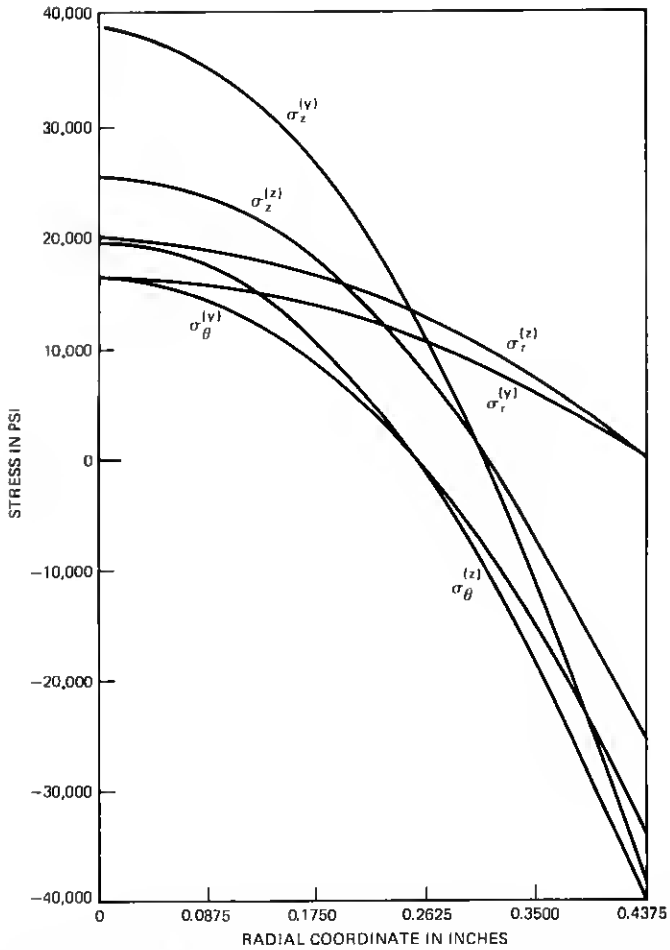

Fig. 12—Thermal stress comparison z-growth and y-growth (at $\theta = 45°$) $LiTaO_3$ crystals—long-cylinder method.

were excellent between the two methods described in this paper for z-growth $LiTaO_3$ crystals (isotropic in the plane of the circle) during the post-growth cooling stage (Fig. 11). Comparisons of thermal stresses between a y-(or x-) growth $LiTaO_3$ crystal (both anisotropic in the plane of the circle) and a z-growth crystal are presented (Fig. 12). Differences in the stress distributions were not great enough to favor either growth direction; the more important consideration is to slow the cooling process down enough to keep radial thermal gradient to a minimum.

VII. ACKNOWLEDGMENT

The author gratefully acknowledges B. E. Nevis for his critical review of this paper and his assistance in estimating rational thermal gradients during the cooling stage of the lithium tantalate crystal.

APPENDIX

Stress-Strain Relationships—Long Cylinder

The most general stress-strain relationship considered is the 4 × 4 submatrix bounded by the dotted lines of eq. (18) as shown below, with no coupling between the stresses (σ_x, σ_y, σ_z, τ_{xy}) and the strains (γ_{yz}, γ_{zx}).

$$\begin{Bmatrix} \sigma_x \\ \sigma_y \\ \sigma_z \\ \tau_{xy} \\ \\ \tau_{yz} \\ \tau_{zx} \end{Bmatrix} = \left[\begin{array}{cccc:cc} C_{xx} & C_{xy} & C_{xz} & 0 & 0 & 0 \\ C_{xy} & C_{yy} & C_{yz} & 0 & 0 & 0 \\ C_{xz} & C_{yz} & C_{zz} & 0 & 0 & 0 \\ 0 & 0 & 0 & C_{ss} & 0 & 0 \\ \hdashline 0 & 0 & 0 & 0 & & \\ 0 & 0 & 0 & 0 & & \end{array}\right] \begin{Bmatrix} \epsilon_x \\ \epsilon_y \\ \epsilon_z \\ \gamma_{xy} \\ \\ \gamma_{yz} \\ \gamma_{zx} \end{Bmatrix}. \tag{18}$$

After inclusion of thermal strains, eq. (18) can be restated as

$$\{\sigma_0\} = [C_0]\left(\{\epsilon_0\} - \left\{\int \alpha dT\right\}\right), \tag{19}$$

where

$$\{\sigma_0\} = \{\sigma_x\ \sigma_y\ \sigma_z\ \tau_{xy}\},$$
$$\{\epsilon_0\} = \{\epsilon_x\ \epsilon_y\ \epsilon_z\ \gamma_{xy}\},$$
$$\left\{\int \alpha dT\right\} = \left\{\int \alpha_x dT\ \int \alpha_y dT\ \int \alpha_z dT\ 0\right\},$$

and $[C_0]$ is the 4 × 4 submatrix of eq. (18).

Now consider a rotation about z by the angle θ, and let $\{\sigma_a\} = \{\sigma_r\ \sigma_\theta\ \sigma_z\ \tau_{r\theta}\}$ be the radial, tangential, longitudinal, and shear stress, respectively. The relationship between this rotated stress field and $\{\sigma_0\}$ can be expressed as

$$\{\sigma_a\} = [B]\{\sigma_0\}, \tag{20}$$

where

$$[B] = \begin{bmatrix} \cos^2\theta & \sin^2\theta & 0 & 2\sin\theta\cos\theta \\ \sin^2\theta & \cos^2\theta & 0 & -2\sin\theta\cos\theta \\ 0 & 0 & 1 & 0 \\ -\sin\theta\cos\theta & \sin\theta\cos\theta & 0 & \cos^2\theta - \sin^2\theta \end{bmatrix}.$$

Conjugate to eq. (20) is the following relationship between tbe strains

$$\{\epsilon_0\} = [B]^t\{\epsilon_a\}, \tag{20a}$$

where

$$\{\epsilon_a\} = \{\epsilon_r\ \epsilon_\theta\ \epsilon_z\ \gamma_{r\theta}\}.$$

Eqs. (19), (20), and (20a) can be combined as

$$\{\sigma_a\} = [C_a]\{\epsilon_a\} - [B][C_0]\{\alpha dT\}, \tag{21}$$

where

$$[C_a] = [B][C_0][B]^t.$$

After multiplying eq. (21) by $[C_a]^{-1}$ and rearranging, the following result is obtained.

$$\{\epsilon_a\} = [E]\{\sigma_a\} + ([B]^t)^{-1}\left\{\int \alpha dT\right\}, \tag{22}$$

wbere

$$[E] = [C_a]^{-1} = ([B]^t)^{-1}[C_0]^{-1}[B]^{-1}. \tag{22a}$$

Tentatively, let $\epsilon_z = 0$. This results in a longitudinal stress applied at the ends of tbe cylinder. From the third line of eq. (22), the longitudinal stress can be obtained as

$$\sigma_z = 1/E_{33}\left(E_{31}\,\sigma_r + E_{32}\,\sigma_\theta + E_{34}\,\tau_{r\theta} + \int \alpha_z dT\right), \tag{23}$$

where, from eq. (22a),

$$\begin{aligned} E_{31} &= E_{xz}\cos^2\theta + E_{yz}\sin^2\theta, \\ E_{32} &= E_{xz}\sin^2\theta + E_{yz}\cos^2\theta, \\ E_{33} &= E_{zz}, \\ E_{34} &= 2\sin\theta\cos\theta\,(E_{yz} - E_{xz}), \end{aligned}$$

and E_{zz}, E_{yz}, and E_{zz} are obtained from $[C_0]^{-1}$.

From eq. (23) we obtain

$$\{\sigma_a\} = [D]\{\sigma_b\} - \left\{0\ 0\ \ 1/E_{33}\int \alpha_z dT\ \ 0\right\}, \tag{24}$$

where

$$\{\sigma_b\} = \{\sigma_r\ \sigma_\theta\ \tau_{r\theta}\}$$

and

$$[D] = \begin{Bmatrix} 1 & 0 & 0 \\ 0 & 1 & 0 \\ -E_{31}/E_{32} & -E_{32}/E_{33} & -E_{34}/E_{33} \\ 0 & 0 & 1 \end{Bmatrix}.$$

After substituting eq. (24) into eq. (22) and premultiplying by $[D]^t$ (remember $\epsilon_z = 0$), we obtain

$$\{\epsilon_b\} = [E_b]\{\sigma_b\} + [B_b]\left\{\int \alpha dT\right\}, \tag{25}$$

where

$$\{\epsilon_b\} = \{\epsilon_r\ \epsilon_\theta\ \gamma_{r\theta}\},$$
$$[E_b] = [D]^t[E][D]$$

and

$$[B_b] = [D]^t([B]^t)^{-1}$$
$$= \begin{Bmatrix} \cos^2\theta & \sin^2\theta & -E_{31}/E_{33} & \sin\theta\cos\theta \\ \sin^2\theta & \cos^2\theta & -E_{32}/E_{33} & -\sin\theta\cos\theta \\ -2\sin\theta\cos\theta & 2\sin\theta\cos\theta & -E_{34}/E_{33} & \cos^2\theta - \sin^2\theta \end{Bmatrix}.$$

Let $[C] = [E_b]^{-1}$. After inverting eq. (25) we obtain a desired result.

$$\{\sigma_b\} = [C]\left(\{\epsilon_b\} - [B_b]\left\{\int \alpha dT\right\}\right) \tag{26}$$

subject to the restriction $\epsilon_z = 0$, which will be removed after an initial solution is obtained.

REFERENCES

1. R. W. Clough, F. Asce, and Y. Rashid, "Finite Element Analysis of Axi-Symmetric Solids," JEMD of ASME, *EM1*, 1965, pp. 71–85.
2. E. L. Wilson, "Structural Analysis of Axisymmetric Solids," JAIAA, 1965, pp. 2269–2274.
3. S. P. Timoshenko and J. N. Goodier, *Theory of Elasticity*, 2nd Edition, New York: McGraw-Hill 1951, pp. 60, 65–66, 408–410.
4. A. W. Warner, M. Onoe, and G. A. Coquin, "Determination of Elastic and Piezoelectric Constants for Crystals in Class (3m)," J. Acoust. Soc. Amer., *6*, 1967, pp. 1223–1231.
5. H. Iwasaki, S. Miyagawa, T. Yamada, N. Uchida, and N. Niizeki, "Single Crystal Growth and Physical Properties of $LiTaO_3$," Rev. Elec. Commun. Laboratories (Japan), *20*, January–Feburary, 1972, pp. 129–137.